

IV. *RNF213*発見以前の遺伝研究

上述のとおり、地域・人種偏在性、一部で家族歴を認めること、一卵性双生児での高い表現型一致率などから、遺伝的因子の関与は従来から疑われてきた^{36, 40, 48)}。そのため、病理学的な検討とともに遺伝研究も精力的に行われてきた。

もやもや病家系の調査に基づく連鎖解析が、1999年にIkedaらにより初めて報告された²¹⁾。その後もわが国において複数の連鎖解析が実施され、3p24.2-p26, 6q25, 8q23, 12p12, 17q25の5つの候補染色体領域が示された^{24, 50, 58)}。また、候補領域6q25の発見を受けて、HLA遺伝子型との相関解析も日本や韓国、ヨーロッパで行われているが、HLA-DRB1*13が韓国とヨーロッパにて高い相関が示された以外は、一致した結果が得られていない^{3, 12, 16, 25, 30, 34)}。さらに、これらの国で*TIMP2*, *PDGFRB*, *TGFBI* 遺伝子多型が相関するという報告もあるが^{29, 49)}、その後、再現性のある結果が得られていない³⁸⁾。

Mineharuらは15の大家系を解析した結果、家族性もやもや病は浸透率（遺伝因子をもっている個体が、疾患を発症する率）の低い常染色体優性遺伝形式をとることを示した⁴⁰⁾。また、常染色体劣性遺伝形式をとる家系も報告されているが^{21, 47)}、どのような遺伝形式でも、家族例では女性の比率が高くなっている。

V. *RNF213*の発見

2011年、2つの独立した研究グループが異なる解析手法により、日本人におけるもやもや病感受性遺伝子として、染色体17q25.3に存在する*RNF213*を同定した。東北大学の研究グループは

72名の患者でGWASおよびlocus-specific association studyを行った²⁸⁾。京都大学の研究グループは、8家系を用いた全ゲノム連鎖解析の後、8名のindex caseにて全エクソーム解析を行った³⁷⁾。

その結果、両研究において*RNF213*の遺伝子多型p.R4810K [c.14576G>A, rs112735431などと表記されることもある。*RNF213*の塩基配列で14576番目の塩基グアニン (G) がアデニン (A) に変わり、遺伝子産物のアミノ酸配列で4810番目のアルギニン (R) がリシン (K) となる変異を同定した。また、相関解析にて*RNF213* p.R4810Kは日本人患者の90%、韓国人患者の79%、中国人患者の23%に認め、健常人に対するオッズ比はそれぞれ340倍、136倍、15倍であった³⁷⁾。Caucasian人種のもやもや病患者では、この多型は認められなかった。一方で、これら東アジアの健常者集団の2~3%にも同変異を認めた(図1)。さらにMiyawakiらは、同変異が動脈硬化性脳血管狭窄症とも関連していることを示した(変異保有率:23.8%)⁴³⁾。最近の報告では、アメリカにおける*RNF213* p.R4810Kの保有率は、アジア系アメリカ人で56%に対し、非アジア系で3.6%であり、アジア系で高い⁶⁾。また*RNF213*発見当初より、東アジア、欧米を含め、p.R4810K以外の*RNF213* rare variantも報告されている^{6, 37, 45)}。

このように*RNF213*は、もやもや病有病率の世界的な地域・人種偏在性、疾患の世代間伝達(広い意味で、もやもや病は遺伝し得ることを論理的に説明できる歴史的な発見となった。またMiyatakeらの報告では*RNF213* p.R4810Kホモ変異型が全患者の約7%に認められ、ヘテロ変異型よりも、発症が若年で(それぞれ中央値3歳, 7歳),

経過も重症となる傾向にあり、*RNF213* p.R4810Kの臨床的なバイオマーカーとしての意義が示された⁴²⁾。

*RNF213*はユビキチンリガーゼ活性をもつring finger domainと2つのAAA+ ATPase module (Walker AおよびBモチーフ) から構成される591kDaの蛋白をコードする^{37, 44)}。In vitroでの機能解析では*RNF213*変異は転写レベルやユビキチン活性に変化をきたさなかったが、*RNF213*をknockdownしたzebrafishにおいて、頭部(眼動脈)の血管形成に異常を認めた。*RNF213* knockoutマウスによる解析では、生理的条件下およびtransient middle cerebral artery occlusion (tMCAO) モデルにおいて、頭蓋内血管の異常は再現されていない^{26, 52)}。ただし、正常マウスと比較して、虚血負荷後の血流改善が良好で、MMP-9発現が増加したという結果から、*RNF213*変異が血管新生の亢進、すなわちヒトでいうもやもや血管の発達に関連する可能性が示された。またこの結果は、もやもや病が*RNF213*変異単独では発症しないが、環境因子など二次的因子の関与によって生じる多因子疾患であることの傍証ともなった^{26, 51, 52)}。

RNF213 p.R4810Kを有する患者から作製したiPS細胞から誘導した内皮細胞では、tube formation assayでの血管形成能が低下していることが示された¹³⁾。本研究では、もやもや病と血管内皮細胞の機能異常の関連が初めて示された点で意義が高い。さらに*RNF213* p.R4810Kの強制発現を行うと、同様に血管形成能の低下を示したが、siRNAにより変異型*RNF213*の発現を抑制すると、血管形成能に変化は認めなかった。このことから*RNF213* p.R4810Kの影響はgain of function

(*RNF213*変異により産生される異常蛋白質が、疾患の原因となる)形式であることが示唆される。

また、この血管形成能の低下には細胞分裂に関連する蛋白質Securinの抑制が関与することが示された。さらに*RNF213* p.R4810Kは細胞分裂の異常や染色体異数性の増加といったゲノム不安定性をきたすことも明らかになっている¹⁴⁾。Kobayashiらによる最近の報告では、内皮細胞においてIFN- β 刺激が*RNF213*の発現を誘導し、血管新生能を低下させた³²⁾。*RNF213* p.R4810Kの強制発現ではIFN- β 刺激なしでも、血管新生能の低下をきたした。また、内皮細胞特異的に*RNF213* p.R4757K (p.R4810K ortholog: ヒトの*RNF213* p.R4810Kに相当するマウスの遺伝子多型)を強制発現させたトランスジェニック (Tg) マウスでも低酸素下において脳血管新生の抑制を認めた。分子構造学的には*RNF213* p.R4810KがWalker BモチーフのATPase活性を低下させ、*RNF213*の多量体形成を安定化させることで、血管新生能低下につながることを示唆された。一方、AAA+欠損では多量体が形成されず、血管新生能に変化は認めなかった。このことは、やはり変異の影響がgain of function形式であることと矛盾しない。感染症や自己免疫性疾患、炎症性疾患では、IFN- β が増加することから、これらの二次的ないし環境因子として発症に関与する可能性が実験的に示唆されたことになる。また、*RNF213* p.R4810Kを保有すると低酸素に対する感受性に異常をもつ可能性も示された。ただし、上記のTgマウスにおいても頭蓋内血管狭窄やもやもや血管は再現されておらず、かつ血管新生能の低下は疾患の臨床像と必ずしも単純に一致しないため、さらなる究明が待たれる(図2)。

VI. *RNF213*発見以降（エピジェネティクスの観点を中心に）

表現型不一致（一方がもやもや病を発症し、もう一方は正常な脳血管を持つ）一卵性双生児の存在や、健常集団における*RNF213*変異保因率と実際の有病率の乖離は、*RNF213*だけではもやもや病の発症を完全には説明できないことを示している。上述のような*RNF213*変異の生理学的意義の解明や、*RNF213*以外の遺伝的素因探索の他にも、病態解明に向けた新たな展開として、エピゲノムに関する研究が始められている。

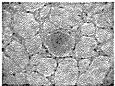
エピゲノムとは、DNA配列の変化を伴わずに、細胞分裂後も継承される遺伝子発現調節機構のことで、エピジェネティクスとはその学問領域を指す⁵⁾。DNAメチル化やヒストン修飾などが代表的な機構とされ、microRNA (miRNA) による遺伝子発現制御もこれに加えられることがある。エピゲノムは細胞・組織特異的な遺伝子発現に寄与し、生理的に極めて重要な役割を果たす。加齢や感染、炎症などの環境要因も、エピゲノム異常の誘因となることがわかっている。さらに、その

異常が、腫瘍、代謝性疾患、精神・神経疾患、免疫疾患、心血管疾患といった多くの疾患に関与することも近年明らかにされつつある。

miRNAは20塩基前後の短いnon-coding RNAで、特定のmRNAに作用し、遺伝子発現を抑制的に制御する。現在、ヒトにおいては2,000種類以上のmiRNAがデータベースに登録されている。一つのmiRNAが複数のmRNAを標的とすることで、多くの生理的プロセスの細かな制御にかかわり、他のエピゲノム機構と同様に、その異常が複数の疾患と関連していることが報告されてきている³³⁾。また、細胞から分泌されたmiRNA (circulating miRNA) が血中で安定に存在するため、疾患バイオマーカーとしての役割が近年注目されている⁴¹⁾。もやもや病においてもmiRNAの関与が報告され始めており、Daiらは、もやもや病患者において発現が変動している複数の血清中miRNAが存在していることを示した⁷⁾。またbioinformatics解析により、それらが*RNF213*や*BRCC3*を標的とし、血管新生に影響を与えている可能性を示した。Zhaoらは、血清中のlet-7 familyの発現が、もやもや病患者で増加しており、

RNF213

- Knockdown zebrafish : 血管形成異常
- Knockout マウス : 頭蓋内血管異常 (-), 虚血負荷後血流改善 ↑
- 内皮細胞



- ✓ p.R4810K (患者) : 血管形成能 ↓
- ✓ p.R4810K 強制発現 : 血管形成能 ↓
- ✓ *RNF213* 抑制 (siRNA) : 血管形成能 →

}

gain of function

Tube formation assay ✓ IFN-β刺激⇒*RNF213*発現⇒血管形成能 ↓

- p.R4810K Tg マウス : 脳血管新生 ↓ (低酸素下)
 - ✓ 頭蓋内血管狭窄 / もやもや血管 (-)
 - ✓ 血管新生 ↓ ≠ 臨床像?

図2 *RNF213*の生理的機能に関する研究のまとめ

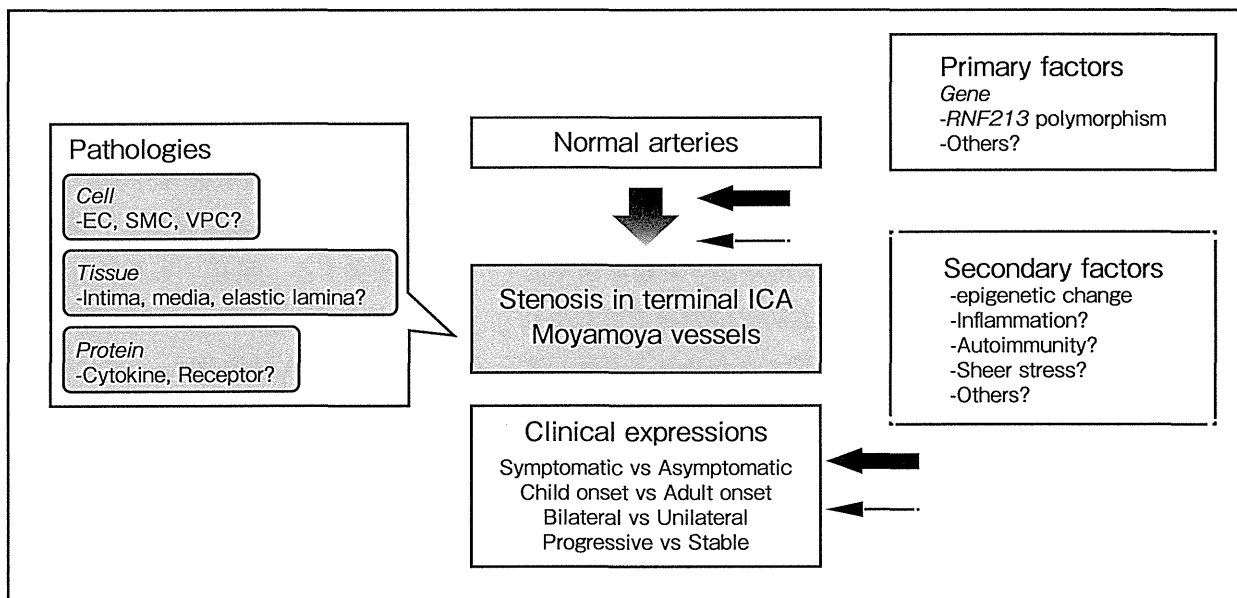


図3 もやもや病発症の推定機序

もやもや病では、*RNF213*多型に加え、発症のトリガーとして、何らかの二次的因子が想定される。さらに*RNF213*多型以外にも発症にかかわる一次的因子の存在も否定できない。また、これらの因子が、血管狭窄の進行、もやもや血管の発達に加え、多様な臨床型の形成に関与していると推測される。

EC : endothelial cell, SMC : smooth muscle cell, VPC : vascular progenitor cell, ICA : internal carotid artery

特にlet-7cは*RNF213*の発現を抑制することを実験的に明らかにした⁶⁰⁾。

miRNAの発現は病勢などに応じてダイナミックに変化するものや、あるいは小児期から成人期にかけて一定しているものが存在する可能性がある。そうしてmiRNAがもやもや病の発症および病態修飾因子となることは十分考えられる。

VII. 最後に

*RNF213*の発見、その後の研究により、この数年でもやもや病の病態解明に向け大きく前進していると言える。*RNF213*が発症に大きく関与していることは間違いなく、さらなる研究が必要である。ただし欧米人では変異保因者自体が少なく³⁷⁾、2013年に行われたGWASでも*RNF213*を含め感受性遺伝子の発見に至っていない³⁸⁾。東ア

ジアにおいても*RNF213*変異保因者がすべて発症するわけではないという事実は、*RNF213*以外の素因遺伝子の存在、エピゲノムを含めた二次的因子の関与が想定される。

もやもや病の発病機序に関して、two hit theoryが以前より提案されているが¹⁸⁾、primary factorとして*RNF213*以外の要因も想定され得るし、何らかのsecondary factorがトリガーとなっている可能性がある(図3)。さらには“two hit”とは限らず、“multiple hit”である可能性もあるだろう。疾患の本態が内皮細胞にあるのか、もしくは平滑筋細胞、あるいはそれらの前駆細胞にあるのかについても、結論は得られていない。本稿で詳細は述べなかったが、内皮細胞へのshear stressの関与、内頸動脈終末部という血行力学的な位置的特異性、血栓形成要因の関与など、まったく別

の観点に基づく疾患原因の推定も行われている。また一部の類もやもや病（もやもや症候群）の病態解析に基づき、もやもや病の原因推定を進める研究も以前から試みられている¹¹⁾。

いずれにしても、“なぜ内頸動脈終末部に進行

性狭窄が起こるのか？”は、今なお本疾患最大の疑問である。今後、これらが解明されることで、もやもや病の診断、治療、ひいては予防に大きな革新がもたらされることを期待したい。

文献

- 1) Achrol AS, Guzman R, Lee M, Steinberg GK: Pathophysiology and genetic factors in moyamoya disease. *Neurosurg Focus* 26: E4, 2009
- 2) Ahn IM, Park DH, Hann HJ, et al: Incidence, prevalence, and survival of moyamoya disease in Korea: a nationwide, population-based study. *Stroke* 45: 1090-5, 2014
- 3) Aoyagi M, Ogami K, Matsushima Y, et al: Human leukocyte antigen in patients with moyamoya disease. *Stroke* 26: 415-7, 1995
- 4) Baba T, Houkin K, Kuroda S: Novel epidemiological features of moyamoya disease. *J Neurol Neurosurg Psychiatry* 79: 900-4, 2008
- 5) Bird A: Perceptions of epigenetics. *Nature* 447: 396-8, 2007
- 6) Cecchi AC, Guo D, Ren Z, et al: RNF213 rare variants in an ethnically diverse population with Moyamoya disease. *Stroke* 45: 3200-7, 2014
- 7) Dai D, Lu Q, Huang Q, et al: Serum miRNA signature in Moyamoya disease. *PLoS One* 9: e102382, 2014
- 8) Fukui M, Kono S, Sueishi K, et al: Moyamoya disease. *Neuropathology* 20 (Suppl) : S61-4, 2000
- 9) Goto Y, Yonekawa Y: Worldwide distribution of moyamoya disease. *Neurol Med Chir (Tokyo)* 32: 883-6, 1992
- 10) Graham JF, Matoba A: A survey of moyamoya disease in Hawaii. *Clin Neurol Neurosurg* 99 (Suppl 2) : S31-5, 1997
- 11) Guey S, Tournier-Lasserre E, Herve D, et al: Moyamoya disease and syndromes: from genetics to clinical management. *Appl Clin Genet* 8: 49-68, 2015
- 12) Han H, Pyo CW, Yoo DS, et al: Associations of Moyamoya patients with HLA class I and class II alleles in the Korean population. *J Korean Med Sci* 18: 876-80, 2003
- 13) Hitomi T, Habu T, Kobayashi H, et al: Downregulation of Securin by the variant RNF213 R4810K (rs112735431, G>A) reduces angiogenic activity of induced pluripotent stem cell-derived vascular endothelial cells from moyamoya patients. *Biochem Biophys Res Commun* 438: 13-9, 2013
- 14) Hitomi T, Habu T, Kobayashi H, et al: The moyamoya disease susceptibility variant RNF213 R4810K(rs112735431) induces genomic instability by mitotic abnormality. *Biochem Biophys Res Commun* 439: 419-26, 2013
- 15) Hojo M, Hoshimaru M, Miyamoto S, et al: Role of transforming growth factor-beta 1 in the pathogenesis of moyamoya disease. *J Neurosurg* 89: 623-9, 1998
- 16) Hong SH, Wang KC, Kim SK, et al: Association of HLA-DR and -DQ Genes with Familial Moyamoya Disease in Koreans. *J Korean Neurosurg Soc* 46: 558-63, 2009
- 17) Hoshino H, Izawa Y, Suzuki N; Research Committee on Moyamoya Disease: Epidemiological features of moyamoya disease in Japan. *Neurol Med Chir (Tokyo)* 52: 295-8, 2012
- 18) Houkin K, Ito M, Sugiyama T, et al: Review of past research and current concepts on the etiology of moyamoya disease. *Neurol Med Chir (Tokyo)* 52: 267-77, 2012
- 19) Houkin K, Nakayama N, Kuroda S, et al: Novel magnetic resonance angiography stage grading for moyamoya disease. *Cerebrovasc Dis* 20: 347-54, 2005
- 20) Houkin K, Yoshimoto T, Abe H, et al: Role of basic fibroblast growth factor in the pathogenesis of moyamoya disease. *Neurosurg Focus* 5: e2, 1998
- 21) Ikeda H, Sasaki T, Yoshimoto T, et al: Mapping of a familial moyamoya disease gene to chromosome 3p24.2-p26. *Am J Hum Genet* 64: 533-7, 1999
- 22) Ikeda K, Iwasaki Y, Kashihara H, et al: Adult moyamoya disease in the asymptomatic Japanese population. *J Clin Neurosci* 13: 334-8, 2006
- 23) Im SH, Cho CB, Joo WI, et al: Prevalence and epidemiological features of moyamoya disease in Korea. *J Cerebrovasc Endovasc Neurosurg* 14: 75-8, 2012
- 24) Inoue TK, Ikezaki K, Sasazuki T, et al: Linkage analysis of moyamoya disease on chromosome 6. *J Child Neurol* 15: 179-82, 2000
- 25) Inoue TK, Ikezaki K, Sasazuki T, et al: DNA typing of HLA in the patients with moyamoya disease. *Jpn J Hum Genet* 42: 507-15, 1997
- 26) Ito A, Fujimura M, Niizuma K, et al: Enhanced post-ischemic angiogenesis in mice lacking RNF 213; a susceptibility gene for moyamoya disease. *Brain Res* 1594: 310-20, 2015
- 27) Kaku Y, Morioka M, Ohmori Y, et al: Outer-diameter narrowing of the internal carotid and middle cerebral arteries in moyamoya disease detected on 3D constructive interference in steady-state MR image: is arterial constrictive remodeling a major pathogenesis? *Acta Neurochir (Wien)* 154: 2151-7, 2012
- 28) Kamada F, Aoki Y, Narisawa A, et al: A genome-wide association study identifies RNF213 as the first Moyamoya disease gene. *J Hum Genet* 56: 34-40, 2011
- 29) Kang HS, Kim SK, Cho BK, et al: Single nucleotide polymorphisms of tissue inhibitor of metalloproteinase

- genes in familial moyamoya disease. *Neurosurgery* 58 : 1074-80; discussion 1074-80, 2006
- 30) Kitahara T, Okumura K, Semba A, et al: Genetic and immunologic analysis on moya-moya. *J Neurol Neurosurg Psychiatry* 45: 1048-52, 1982
 - 31) Kleinlog R, Regli L, Rinkel GJ, et al: Regional differences in incidence and patient characteristics of moyamoya disease: a systematic review. *J Neurol Neurosurg Psychiatry* 83: 531-6, 2012
 - 32) Kobayashi H, Matsuda Y, Hitomi T, et al: Biochemical and Functional Characterization of RNF 213 (Mysterin) R4810K, a Susceptibility Mutation of Moyamoya Disease, in Angiogenesis In Vitro and In Vivo. *J Am Heart Assoc* 4: e002146, 2015
 - 33) Koutsis G, Siasos G, Spengos K: The emerging role of microRNA in stroke. *Curr Top Med Chem* 13: 1573-88, 2013
 - 34) Kraemer M, Horn PA, Roder C, et al: Analysis of human leucocyte antigen genes in Caucasian patients with idiopathic moyamoya angiopathy. *Acta Neurochir (Wien)* 154: 445-54, 2012
 - 35) Kuriyama S, Kusaka Y, Fujimura M, et al: Prevalence and clinicoepidemiological features of moyamoya disease in Japan: findings from a nationwide epidemiological survey. *Stroke* 39: 42-7, 2008
 - 36) Kuroda S, Houkin K: Moyamoya disease: current concepts and future perspectives. *Lancet Neurol* 7: 1056-66, 2008
 - 37) Liu W, Morito D, Takashima S, et al: Identification of RNF 213 as a susceptibility gene for moyamoya disease and its possible role in vascular development. *PLoS One* 6: e22542, 2011
 - 38) Liu W, Senevirathna ST, Hitomi T, et al: Genomewide association study identifies no major founder variant in Caucasian moyamoya disease. *J Genet* 92: 605-9, 2013
 - 39) Masuda J, Ogata J, Yutani C: Smooth muscle cell proliferation and localization of macrophages and T cells in the occlusive intracranial major arteries in moyamoya disease. *Stroke* 24: 1960-7, 1993
 - 40) Mineharu Y, Takenaka K, Yamakawa H, et al: Inheritance pattern of familial moyamoya disease: autosomal dominant mode and genomic imprinting. *J Neurol Neurosurg Psychiatry* 77: 1025-9, 2006
 - 41) Mitchell PS, Parkin RK, Kroh EM, et al: Circulating microRNAs as stable blood-based markers for cancer detection. *Proc Natl Acad Sci U S A* 105: 10513-8, 2008
 - 42) Miyatake S, Miyake N, Touho H, et al: Homozygous c.14576 G>A variant of RNF 213 predicts early-onset and severe form of moyamoya disease. *Neurology* 78: 803-10, 2012
 - 43) Miyawaki S, Imai H, Shimizu M, et al: Genetic variant RNF213 c.14576G>A in various phenotypes of intracranial major artery stenosis/occlusion. *Stroke* 44: 2894-7, 2013
 - 44) Morito D, Nishikawa K, Hoseki J, et al: Moyamoya disease-associated protein mysterin/RNF 213 is a novel AAA+ ATPase, which dynamically changes its oligomeric state. *Scientific reports* 4: 4442, 2014
 - 45) Moteki Y, Onda H, Kasuya H, et al: Systematic Validation of RNF 213 Coding Variants in Japanese Patients With Moyamoya Disease. *J Am Heart Assoc* 4: e001862, 2015
 - 46) Nanba R, Kuroda S, Ishikawa T, et al: Increased expression of hepatocyte growth factor in cerebrospinal fluid and intracranial artery in moyamoya disease. *Stroke* 35: 2837-42, 2004
 - 47) Nanba R, Kuroda S, Tada M, Ishikawa T, et al: Clinical features of familial moyamoya disease. *Childs Nerv Syst* 22: 258-62, 2006
 - 48) Roder C, Nayak NR, Khan N, et al: Genetics of Moyamoya disease. *J Hum Genet* 55: 711-6, 2010
 - 49) Roder C, Peters V, Kasuya H, et al: Polymorphisms in TGFB 1 and PDGFRB are associated with Moyamoya disease in European patients. *Acta Neurochir (Wien)* 152: 2153-60, 2010
 - 50) Sakurai K, Horiuchi Y, Ikeda H, et al: A novel susceptibility locus for moyamoya disease on chromosome 8 q 2.3. *J Hum Genet* 49: 278-81, 2004
 - 51) Sonobe S, Fujimura M, Niizuma K, et al: Increased vascular MMP- 9 in mice lacking RNF 213 : moyamoya disease susceptibility gene. *Neuroreport* 25: 1442-6, 2014
 - 52) Sonobe S, Fujimura M, Niizuma K, et al: Temporal profile of the vascular anatomy evaluated by 9. 4 -T magnetic resonance angiography and histopathological analysis in mice lacking RNF213: a susceptibility gene for moyamoya disease. *Brain Res* 1552: 64-71, 2014
 - 53) Suzuki J, Takaku A: Cerebrovascular "moyamoya" disease. Disease showing abnormal net-like vessels in base of brain. *Arch Neurol* 20: 288-99, 1969
 - 54) Takekawa Y, Umezawa T, Ueno Y, et al: Pathological and immunohistochemical findings of an autopsy case of adult moyamoya disease. *Neuropathology* 24: 236-42, 2004
 - 55) Takeuchi K, Shimizu K: Hypoplasia of the bilateral internal carotid arteries. *Brain Nerve* 9: 37-43, 1957
 - 56) Uchino K, Johnston SC, Becker KJ, et al: Moyamoya disease in Washington State and California. *Neurology* 65: 956-8, 2005
 - 57) Wakai K, Tamakoshi A, Ikezaki K, et al: Epidemiological features of moyamoya disease in Japan: findings from a nationwide survey. *Clin Neurol Neurosurg* 99 (Suppl 2) : S1-5, 1997
 - 58) Yamauchi T, Tada M, Houkin K, et al: Linkage of familial moyamoya disease (spontaneous occlusion of the circle of Willis) to chromosome 17q25. *Stroke* 31: 930-5, 2000
 - 59) Yonekawa Y, Ogata N, Kaku Y, et al: Moyamoya disease in Europe, past and present status. *Clin Neurol Neurosurg* 99 (Suppl 2) : S58-60, 1997
 - 60) Zhao S, Gong Z, Zhang J, et al: Elevated Serum MicroRNA Let- 7 c in Moyamoya Disease. *J Stroke Cerebrovasc Dis*, 2015

Investigating Brain Network Characteristics Interrupted by Covert White Matter Injury in Patients with Moyamoya Disease: Insights from Graph Theoretical Analysis

Ken Kazumata¹, Khin Khin Tha², Hisashi Narita³, Hideo Shichinohe¹, Masaki Ito¹, Haruto Uchino¹, Takeo Abumiya¹

Chronic ischemia in adult moyamoya disease (MMD) reduces the integrity of normal-appearing white matter (WM). We investigated whether covert WM impairment alters large-scale brain networks and specific neural circuits associated with neurocognitive dysfunction in MMD. Forty-six participants (control, $n = 23$; MMD, $n = 23$) were examined using diffusion tensor imaging and streamline tractography. Structural connectivity among 90 cortical and subcortical brain regions was evaluated using the mean fractional anisotropy along the fiber tracts. Graph theoretical analysis was used to measure network parameters and inter-regional connectivity. Global network parameters were reduced in patients with MMD, including cluster coefficient (controls vs. MMD: 3.62 ± 0.24 vs. 3.26 ± 0.36 ; $P < 0.0001$), characteristic path length (controls vs. MMD: 1.20 ± 0.02 vs. 1.17 ± 0.01 ; $P < 0.001$), and small-world property (controls vs. MMD: 3.07 ± 0.18 vs. 2.83 ± 0.27 ; $P < 0.001$). Reduced pairwise connectivity was found in prefrontal neural circuits within the middle/inferior frontal gyrus; supplementary motor area; and insular, inferior temporal, and dorsal cingulate cortices. Covert WM microstructural changes in patients with MMD alter large-scale brain networks, as well as lateral prefrontal neural circuits. Evaluation of structural connectivity may be useful to assess the severity of chronic ischemic injury from a network perspective.

INTRODUCTION

Moyamoya disease (MMD) is a progressive occlusive cerebral arterial disease characterized by the presence of netlike collaterals at the base of the brain.¹ Chronic hypoperfusion in patients with MMD can develop during childhood, subsequently affecting attention, working memory, and executive function in young- and middle-aged adults, suggesting that information transfer processes have deteriorated by midlife in MMD.²⁻⁵ Reduced cerebral blood flow to the lateral prefrontal cortex is associated with cognitive impairment because the dorsolateral prefrontal cortex, inferior parietal lobule, and intraparietal sulcus form a core network associated with working memory.⁶⁻⁸ Understanding structural changes is crucial for predicting the reversibility of neurocognitive dysfunctions after revascularization surgery. Recently, diffusion tensor imaging (DTI) and voxel-based morphometric analysis have revealed widespread microstructural changes in the white matter (WM), with localized volume reductions in the posterior cingulate in adult patients with MMD.² This implies the disruption of neural pathways plays a pivotal role in the neurocognitive impairments of patients with MMD.²

Although voxel-based analysis has identified regional WM involvement, it has not allowed direct identification of the neural circuits affected in MMD.² Furthermore, alterations in diffusion parameters of WM have been difficult to infer as the brain remodels. Graph theoretical analysis enables the assessment of the structural and functional connectivity of large-scale networks⁹⁻¹¹; hence changes in network parameters have been described in aging, neurodegenerative diseases, epilepsy, and

Key words

- Brain network
- Connectivity
- Diffusion tensor imaging
- Graph theoretical analysis
- Moyamoya disease

Abbreviations and Acronyms

- AAL:** Automated anatomic labeling
- AUC:** Area under the curve
- BC:** Between-ness centrality
- CC:** Clustering coefficient
- DTI:** Diffusion tensor imaging
- FA:** Fractional anisotropy
- FDR:** False discovery rate
- IFG:** Inferior frontal gyrus
- MFG:** Middle frontal gyrus

MMD: Moyamoya disease

NBS: Network-based statistics

TMT: Trail making test

WCST: Wisconsin card sorting test

From the Departments of ¹Neurosurgery, ²Radiobiology and Medical Engineering, and ³Psychiatry, Hokkaido University Graduate School of Medicine, Sapporo, Japan

To whom correspondence should be addressed: Ken Kazumata, M.D., Ph.D.

[E-mail: kazumata@med.hokudai.ac.jp]

Citation: *World Neurosurg.* (2016).

<http://dx.doi.org/10.1016/j.wneu.2015.11.100>

Journal homepage: www.WORLDNEUROSURGERY.org

Available online: www.sciencedirect.com

1878-8750/\$ - see front matter © 2016 Elsevier Inc. All rights reserved.

gliomas.¹²⁻¹⁸ Nevertheless, structural connectivity has rarely been investigated in chronic ischemia. Thus describing the characteristics of brain networks may be useful to expand our knowledge of neurocognitive impairments secondary to chronic ischemia.

Here, we investigated a large-scale network for revealing structural connectivity in controls and adult patients with MMD, using graph theoretical analysis, DTI, and streamline tractography. Graph theoretical analysis was performed to calculate parameters representing network organization as an extension of DTI and streamline tractography, a recently evolved method for analyzing structural connectivity in clinical research.¹⁵ We investigated network characteristics to determine the following: 1) whether covert WM changes can alter whole-brain organization, 2) how diffuse WM involvement can affect specific neural circuits, and 3) whether network parameters correlate with clinical status, as well as neurocognitive examinations.

MATERIAL AND METHODS

Participants

The institutional ethics review board approved the study protocol, and all subjects provided written informed consent before participation. All participants had been subjects in a prior investigation of ours, in which we assessed multiple diffusion tensor parameters and performed voxel-based statistical analyses.² We have described the characteristics of these patients with MMD previously; information is provided in supplementary material.² Twenty-three patients (6 men and 17 women; 21–58 years; mean age, 40.9 ± 9.5 years) were enrolled between April 2012 and April 2014. The control group consisted of 23 subjects (10 men and 13 women; 25–56 years of age; mean age, 39.0 ± 8.1) who had a mean estimated intelligence quotient (IQ) of 108.3 ± 6.6. The inclusion criteria for control subjects were the following: 1) no clinical evidence of psychiatric or neurologic disorders, 2) a normal IQ as assessed by the Japanese version of the Nelson Adult Reading Test, 3) no brain lesions identified on conventional magnetic resonance imaging (MRI) sequences, and 4) no current medication that could affect cognitive function. **Table 1** summarizes the participant characteristics.

A neuropsychologic assessment was undertaken for all patients with MMD studied here, which consisted of a battery sensitive to cognitive dysfunction due to frontal lobe injury/degeneration. Tests included the Wechsler Adult Intelligent Scale, edition 3, Wisconsin Card Sorting test (WCST), Trail Making Test (TMT)—parts A and B, Continuous Performance Task, Stroop test, and Reading span test. Neuropsychologists blinded to the clinical data performed the tests. A detailed description of the neuropsychologic tests and their results is provided in our previous study,² and a brief summary of the neuropsychologic assessments is detailed in supplementary material and **Table 1**.

Image Acquisition and Image Processing

MRI data were acquired using 3.0-T scanner (Achieva TX, Philips Medical Solutions, Best, The Netherlands). Details of scan parameters are provided in **supplementary material**. Data preprocessing procedures were performed using the FMRIB Diffusion Toolbox

Table 1. Subject Demographics and Clinical Characteristics

	Control (n = 23)	MMD (n = 23)	P value
Number of subjects	23	23	—
Age, years ± SD (range)	39.0 ± 8.1 (25-56)	40.9 ± 9.5 (21-58)	0.48
Sex (F/M) (number of subjects)	13/10	17/6	0.35
Risk factor (DM, HT, HL) (number of subjects)	0	5	0.049
Symptoms (number of subjects)			
Asymptomatic	—	13	
TIA	—	10	
Neuropsychologic test			
fiQ			
<80	0%	2 (8.7%)	0.49
TMT-A			
>87	—	3 (13%)	
TMT-B			
>100	—	6 (26%)	
WCST			
CA			
<4	—	7 (30.4%)	
PEM			
>2	—	8 (34.7%)	
PEN			
>3	—	9 (39.1%)	
Stroop			
>10	—	8 (34.8%)	
CPT error			
>3	—	9 (39.1%)	
RST			
<2	—	9 (39.1%)	
MMD, moyamoya disease; SD, standard deviation; fiQ, full-scale intelligent quotient score; TMT, Trail Making Test; WCST, Wisconsin card sorting test; CA, categories achieved; PEM, perseverative errors in Milner; PEN, perseverative errors in Nelson; Stroop, Stroop test; CPT; Conceptual performance task; RST, reading span test.			

(FSL, version 5.0; <http://www.fmrib.ox.ac.uk/fsl>). A detailed description is provided in **supplementary material**.

Construction of Connectivity Matrix

Whole-brain fiber tracking was performed using the fiber assignment by continuous tracking streamline tractography algorithm in the Diffusion toolkit (<http://www.trackvis.org/>).^{19,20} The automated anatomic labeling (AAL) template consisted of 90 cortical and subcortical regions of interest, which were used to construct the connectivity matrix. An adjacency matrix was

obtained by averaging fractional anisotropy (FA) by the volume of the fiber tract connecting region. Connectivity matrices were constructed in MATLAB R2012b (Mathworks, Natick, Massachusetts, USA), using an open-source pipeline package (<http://www.nitrc.org/projects/panda/>).²¹

We employed both weighted adjacency matrices and unweighted adjacency matrices. The former were used to identify group differences in inter-regional connectivity through bivariate analyses, and the latter were used to calculate global and local graph metrics based on complex network analyses.^{9,11,22} There is no clear definition of connectivity in terms of the mean FA along the fiber tract between each pair of nodes. We avoided including extremely spurious connections in calculations by applying thresholds in the connection matrices. The adjacency matrix was thus made binary by applying a threshold to each element of averaged FA, from 0.1–0.35 in 0.01 increments. Using the same cost (density of the nodes) is a common approach to group comparisons. However, because we already know that average FA is lower in MMD than in controls, using the same cost could nullify any subtle decrease in FA for MMD. Therefore we explored the graph measurements for a wide range of thresholds for FA values in each connection.

Graph Theoretical Analysis

Overall network organization and node-specific measures were calculated using the Brain Connectivity Toolbox (BCT; <https://sites.google.com/site/bctnet/>).¹¹ Brief descriptions of each of the network properties are provided in the supplementary material. The clustering coefficient (CC), characteristic path length (L), normalized CC ($\gamma = CC/CC_{rand}$), and characteristic path length ($\lambda = L/L_{rand}$) were computed, where CC_{rand} and L_{rand} represent the average-weighted CC and shortest path length of 100 surrogate random networks with preserved edge weights. The small-world index (σ) was calculated as γ/λ . Modularity (Ci), which quantifies the degree to which the network may be subdivided into delineated groups,¹¹ was calculated by maximizing the number of edges in a subgroup and minimizing the number of edges between subgroups. Degree, local CC, and betweenness centrality (BC) were calculated to examine the local network characteristics of each brain region in the structural network.¹¹

Network-based statistics (NBS) were also used to identify pairs of regions with altered structural connectivity.²² Weighted adjacency matrices were used to express the average FA per volume connecting each pair of nodes in the whole-brain tractography. A detailed description of this statistical procedure has been described elsewhere.²² Briefly, a 2-sample t-test was performed for each pair of regions in the AAL template, on the basis of the hypothesis that the mean value of structural connectivity is equal between groups. Pairs of regions with a t-statistic exceeding a P value of 0.05 (reflecting $t = 1.68$) were identified, as well as the number of edges (connected components). The size of the largest connected component was recorded after a total of 5000 permutations were tested. A corrected P value for each observed component was then calculated using an empirical null distribution of the maximum component size. The 2 hypotheses (controls > MMD and controls < MMD) were evaluated independently. A summary of image processing and analysis is presented in **Figure 1**.

Statistical Analysis

For the global network measures (σ , γ , λ , and Ci), the average of each network property was calculated as the area under the curve (AUC) in the graph generated by the network parameters and FA values used for threshold. AUC values for each network parameter were then compared between groups using a permutation test performed >10,000 times. Statistical significance was defined as $P < 0.05$.

Post-hoc analysis was also performed to explore the altered network properties in regions. We employed a single threshold value of 0.28 because this value yielded the most significant differences in small-world properties (see “Results” later). In the regional analysis, the permutation test was performed 10,000 times for the regional network characteristics (nodal degree, BC, and local cluster coefficient) in all 90 brain regions. To explore possible alterations in regional graph measurements, FDR-uncorrected P values < 0.05 were considered statistically significant. However, because multiple comparisons were performed, the false discovery rate (FDR) was also calculated by Benjamini-Hochberg methods, using the R software package (<https://www.r-project.org/>).²³

The procedure for analyzing local connectivity using NBS is described earlier. Graph metrics were tested for their correlation with neuropsychologic performance. Pearson product-moment correlation analysis was used for associations with the Wechsler Adult Intelligence Scale-III scores (TMT A and B) and permutation tests with >10,000 repetitions for the WCST, Stroop test, continuous performance task, and reading span test. A cutoff value was applied to the last 4 tests. For all comparisons, $P < 0.05$ was considered statistically significant.

RESULTS

Global Network Connectivity

Normalized clustering coefficients (γ) and normalized characteristic path lengths (λ) were lower at all threshold levels in patients with MMD compared with controls (**Figure 2**). Small-world topology ($\sigma > 1$) was observed in both control subjects and patients with MMD (see **Figure 2**). Mean γ , λ , and σ were significantly lower in the MMD than in the control group ($P < 0.01$, **Table 2**). Modularity (Ci) measurements yielded 4 subnetwork communities in each group that included anterior (thalamo-frontal-striatal group) and posterior modules (parietal, temporal, and occipital group) in each hemisphere. However, mean Ci did not reach significance. **Table 2** summarizes the global parameters and statistics.

Local Node-Based Analysis

Next, we performed local node-based analysis using an adjacency matrix at a single FA threshold level of 0.28, where the group difference in σ was significant. In the control subjects, 18 cortical hub regions (top 20%) were revealed in the nodal degrees, including the insula (R, L), hippocampus (R, L), precuneus (R, L), fusiform gyrus (R, L), precentral gyrus (R, L), calcarine sulcus (R, L), anterior and middle cingulum (R, L), and middle frontal gyrus (MFG; R, L). Eleven of 90 nodes in the MMD group exhibited decreased nodal degree, and the right MFG, left MFG, and right precuneus were among the 18 cortical hub regions that exhibited a significant decrease (rt. MFG; $P = 0.003$, lt. MFG; $P = 0.005$, rt.

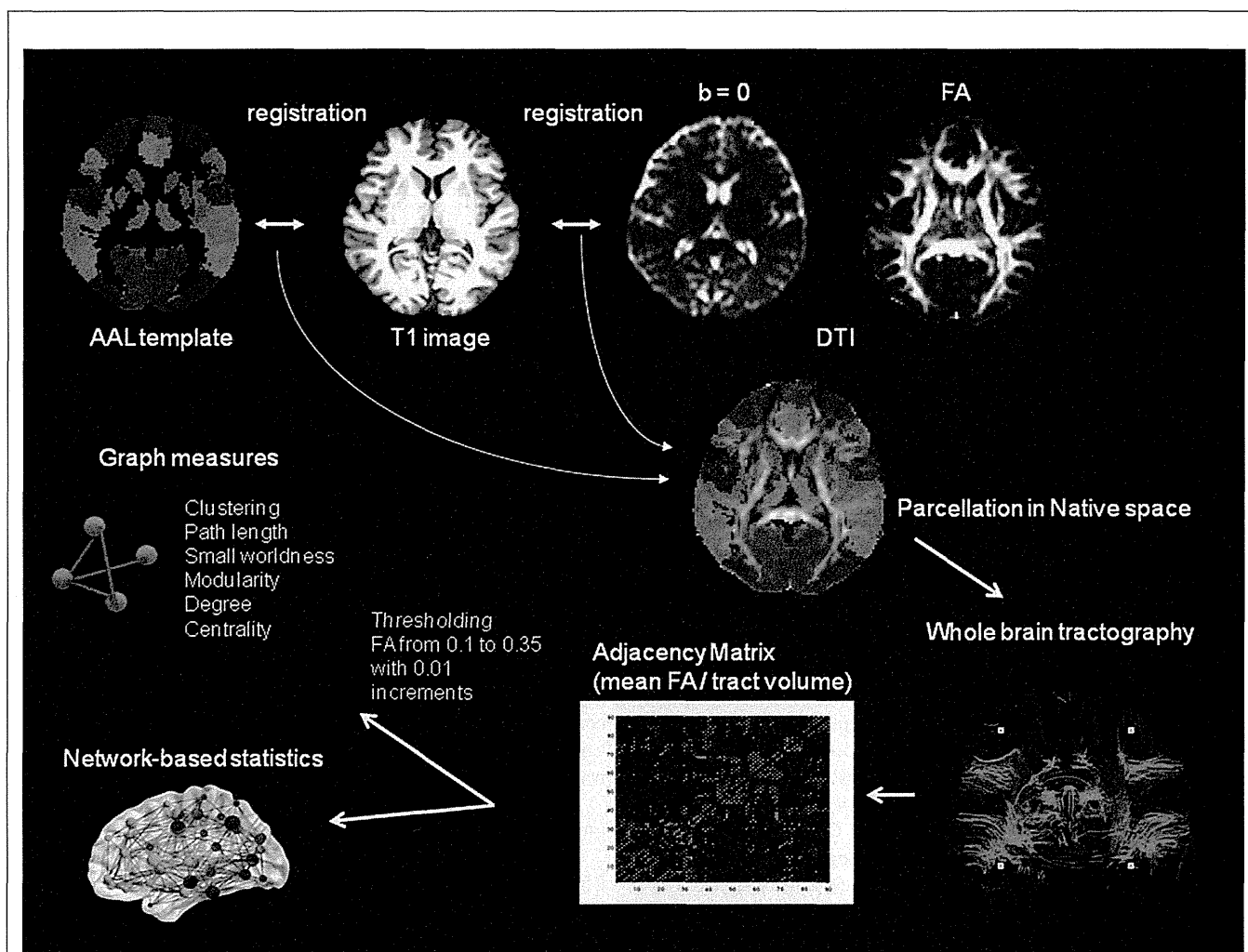


Figure 1. Flow chart for the construction of a white matter network and calculation of graph indices. The illustration was generated from a single subject used in the study. First, an FA image in native space was coregistered to its corresponding T1-weighted image using an affine transformation. The individual T1-weighted image was then nonlinearly registered to the ICBM 152 template. Then, inverse transformation matrix was obtained and applied to an automated anatomical labeling (AAL) template in standard space. The resultant images correspond to a customized AAL template for the individual's native space. Subsequently, for every pair of regions, whole brain deterministic tractography was performed using the Diffusion Toolkit (<http://trackvis.org/dtk/>).

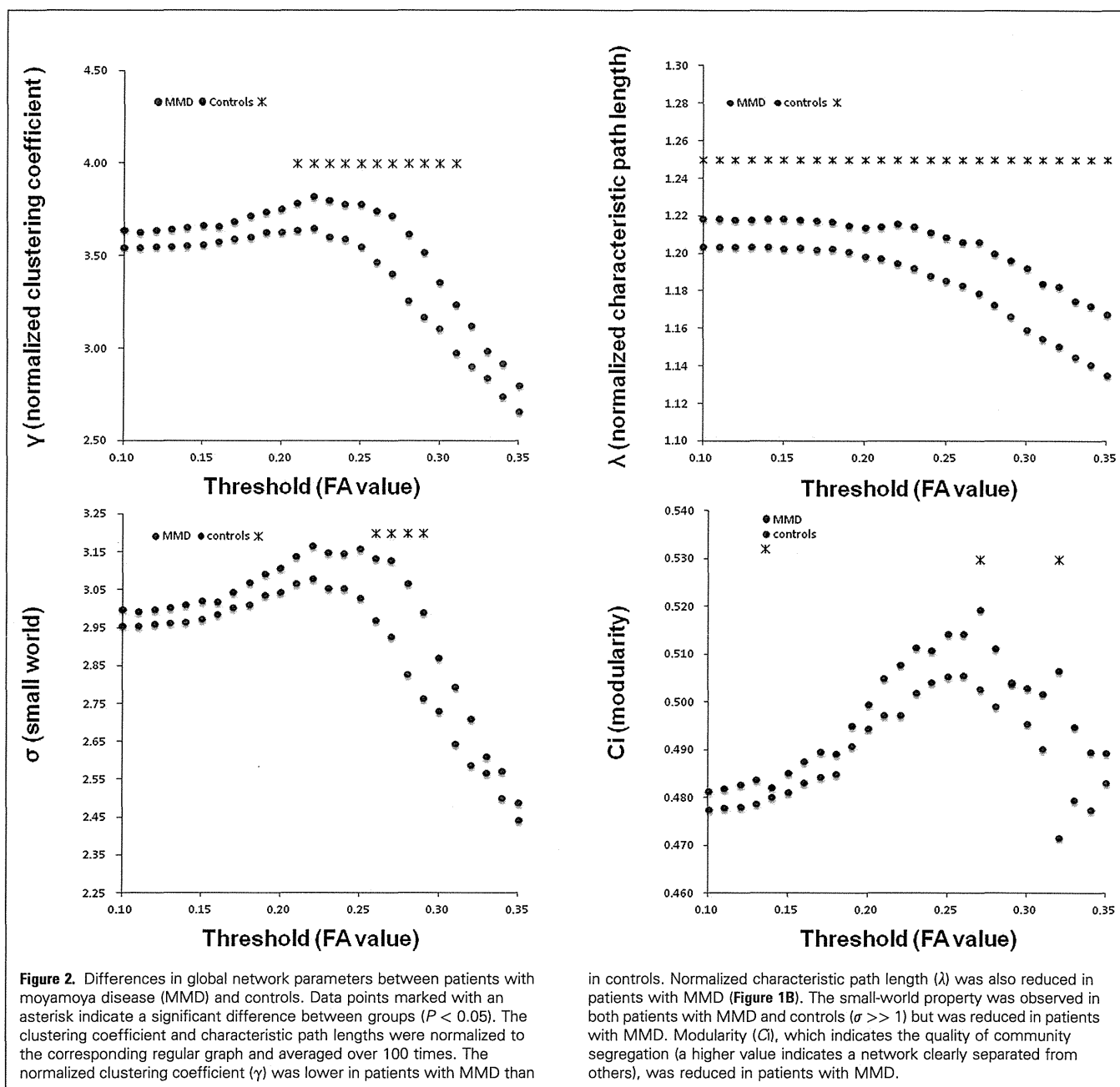
We used the average FA of linking fibers between node i to j . An unweighted adjacency matrix was generated by applying a threshold value to FA from 0.10–0.35 in 0.01 increments, in which the network edges were defined as 1 if the average FA was above the threshold and as 0 otherwise. Overall network characteristics and node-specific organizational characteristics were computed via the Brain Connectivity toolbox (<https://sites.google.com/site/bctnet/>) and compared between patients and healthy controls. The network-based statistics (NBS) approach uses pairwise comparisons to localize specific brain regions in which structural connectivity was altered in patients with moyamoya disease.²²

precuneus; $P = 0.007$; FDR-uncorrected, **Figures 3 and 4**). Five nodes exhibited a significant decrease in BC in the MMD group ($P < 0.05$, FDR-uncorrected): the left and right MFG, left supplementary motor area, right precuneus, and left triangular part of the inferior frontal gyrus (IFG; $P < 0.05$, FDR-uncorrected, see **Figures 3 and 4**; **Table 3**). The regional CC (C) decreased in 14 of the 90 nodes ($P < 0.05$, FDR-uncorrected, see **Figure 3**), and this decrease was observed primarily in the right parieto-occipital region. Additionally, decreased C was observed in nodes of patients with MMD that typically displayed high C values in controls, which

were primarily localized to the posterior part of the brain (see **Figures 3 and 4**). **Table 3** summarizes the local graph measurements.

Network-Based Statistics

NBS identified 3 subnetworks that exhibited reduced inter-regional connectivity in patients with MMD ($P < 0.05$, family-wise error corrected). Network 1 comprised 8 nodes and 7 connections. **Figure 5** illustrates the reduced pairwise connectivity observed in the left MFG-precentral gyrus, precentral gyrus-median cingulum,



MFG-insular, IFG (triangular part, orbital part)—insular, inferior temporal (inferior temporal gyrus, fusiform gyrus)—insular (see Figure 5; Table 4). Network 2 comprised 3 nodes and 2 connections and exhibited reduced connectivity in the right precentral gyrus-IFG (triangular part, rolandic operculum; see Figure 5). Network 3 consisted of 3 nodes and 2 connections, exhibiting reduced connectivity in the superior parietal gyrus—middle occipital gyrus and angular gyrus—middle occipital gyrus (see Figure 5). Pairwise connectivity that was significantly reduced in patients with MMD is summarized in Table 4.

Correlations of Graph Metrics with Neuropsychologic Examinations

In addition to the global graph measures, nodal degree and BC in the MFG were used for the correlation analysis. In addition, the inter-regional connectivity (connectivity strength) of 11 statistically significant edges in NBS analysis was also used to analyze the imaging-neuropsychologic data relationship. The WCST was associated with connectivity between the triangular part of IFG and the left insula ($P = 0.03$). TMT-A was associated with nodal degree in the left MFG ($r = 0.45$; $P < 0.05$), and connectivity strength between the left

Table 2. Complex Network Indices* Revealing Structural Connectivity in Both Controls and Patients with Moyamoya Disease

	Controls	MMD	P value
Small world (σ)	3.07 (0.18)	2.83 (0.27)	0.001
Cluster coefficient (γ)	3.62 (0.24)	3.26 (0.36)	0.0001
Characteristic path length (λ)	1.20 (0.02)	1.17 (0.01)	0.0007
Modularity (C_i)	0.51 (0.01)	0.50 (0.03)	0.079

Network indices were average over each threshold ranged from 0.10 to 0.35.

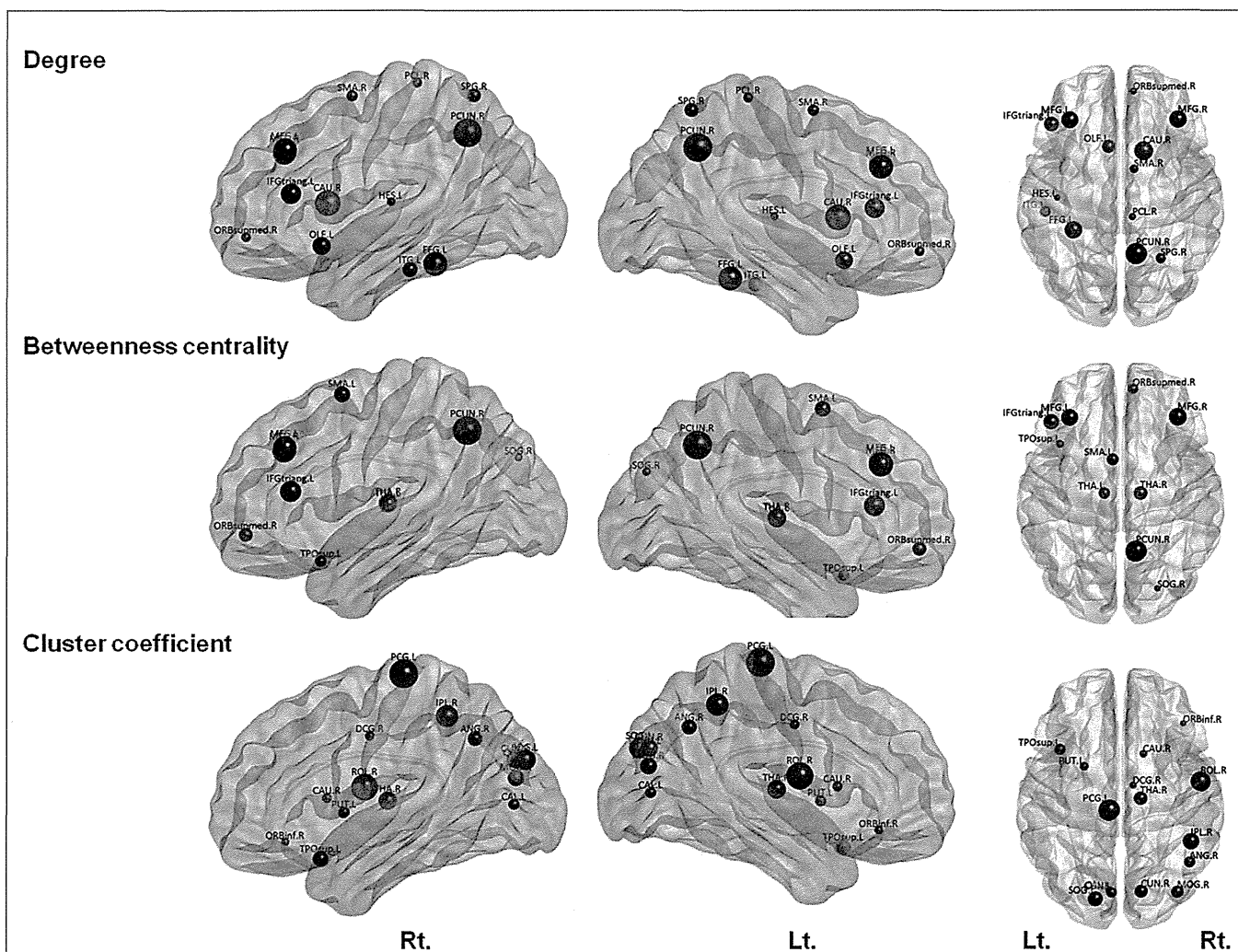


Figure 3. Decreased (*blue*) and increased (*red*) local node measurements in patients with moyamoya disease (MMD), indicating significant between-group differences ($P < 0.05$, uncorrected). The size of each node is proportional to the average value of each parameter (degree, between-ness centrality [BC], and local cluster coefficient) in control subjects. A decrease in degree was observed in the bilateral middle frontal gyrus (MFG), right precuneus (PCUN), inferior frontal gyrus triangular part (IFGtring), supplementary motor area (SMA), paracentral lobule, superior parietal gyrus, Heschl gyrus, olfactory cortex, inferior temporal gyrus, and

fusiform gyrus. An increase in degree was observed in the caudate and superior frontal gyrus medial orbital part (ORBsupmed). Three major connecting nodes (*blue*) demonstrated significant reductions in BC, which refers to a node located in the most frequent path between different regions in patients with MMD. These regions were the left and right MFG, the left SMA, and the left IFGtring and right PCUN ($P < 0.05$, uncorrected). The local cluster coefficient, which refers to the fraction of a node's neighbors that are also neighbors to each other, was reduced in the striatum, thalamus, and parietal-occipital region of patients with MMD.

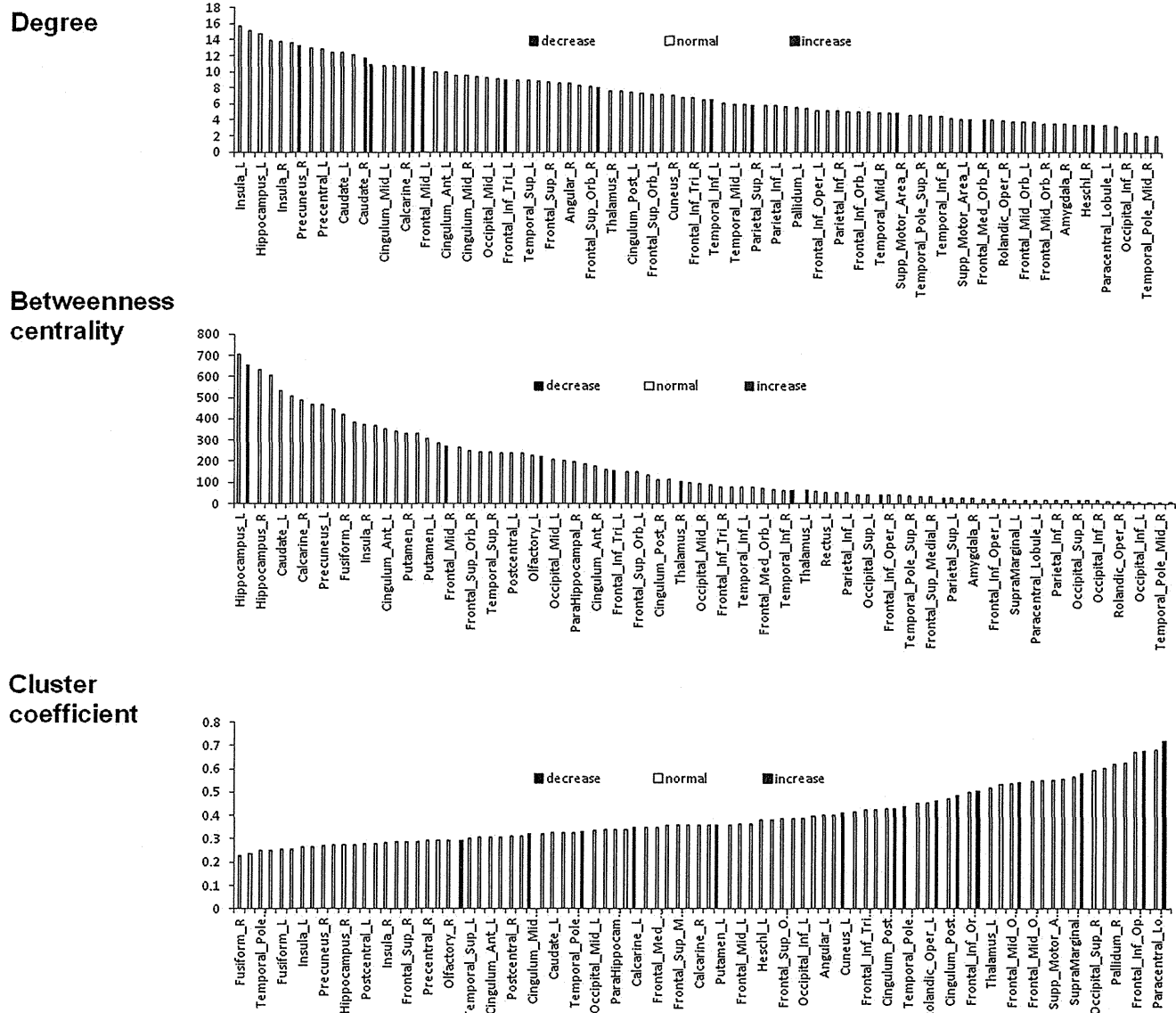


Figure 4. The upper bar graph indicates the mean degree of each area in control subjects and the area exhibiting significant changes in patients with moyamoya disease (MMD). High-degree areas (top 20%) were considered as provincial hubs. The middle bar graph indicates the mean betweenness centrality (BC) in control subjects and areas of impaired BC in patients with MMD. High BC areas (top 20%) were considered as connecting hubs.

Hub-specific reductions have been reported previously in neurodegenerative diseases¹⁵ but were not clear for either provincial hubs (degree) or connecting hubs (BC). Reduced local clustering coefficient (CC) was observed primarily in nonhub regions (regions with a high CC), particularly the superior parietal-occipital region.

precentral and the left MFG ($r = 0.43$; $P < 0.05$). TMT-B was associated with connectivity strength between the left precentral and the left MFG ($r = 0.42$; $P < 0.05$). Finally, TMT A-B was associated with connectivity strength between the left triangular part of the IFG and the left orbital part of the IFG ($r = 0.42$; $P < 0.05$).

DISCUSSION

Adult patients with MMD demonstrate executive dysfunction, attention deficits, and working memory disturbances without

conspicuous ischemic lesions. Covert microstructural changes can develop both in white and gray matter in MMD, which potentially affects interactions with distant brain regions.² We speculated that WM connectivity may change the organization of the entire brain network, as well as specific fiber tracts associated with cognitive functions in patients with MMD. Using graph theoretical analysis, we found that covert microstructural alterations in the WM alter overall brain organization in patients with MMD. Additionally, core neural pathways associated with working memory and

Table 3. Local Graph Measurements

Indices	Regions	Control		MMD		P value	q value
		Mean	SD	mean	SD		
Degree							
Frontal	Paracentral lobule_R	4.0	1.0	2.9	1.0	0.001	0.072
	Supplementary motor area_R	4.8	1.1	3.6	1.3	0.002	0.072
	Middle frontal gyrus_R	10.7	3.4	7.5	3.1	0.003	0.072
	Middle frontal gyrus_L	10.5	3.1	7.9	2.8	0.005	0.085
	Superior frontal gyrus, medial orbital_R	4.0	1.9	5.8	2.9	0.021	0.169
	Inferior frontal gyrus, triangular part	9.0	2.1	7.3	2.8	0.025	0.190
	Olfactory_L	8.0	3.0	6.0	2.0	0.013	0.132
	Inferior temporal gyrus_L	6.5	2.4	4.7	1.7	0.011	0.126
	Heschl gyrus_L	3.3	1.9	2.2	1.3	0.021	0.169
	Fusiform gyrus_L	10.9	3.0	9.0	2.6	0.035	0.244
Parietal	Superior parietal gyrus_R	5.9	2.4	4.1	1.6	0.006	0.085
	Precuneus_R	13.2	2.8	12.4	2.9	0.007	0.085
Subcortical	Caudate_R	11.7	3.0	14.5	2.9	0.003	0.072
BC*							
Frontal	Middle frontal gyrus_R	272.1	206.1	127.0	203.3	0.018	0.353
	Superior frontal gyrus, medial orbital_R	42.7	55.2	94.3	92.3	0.026	0.353
	Supplementary motor area_L	63.5	86.2	23.5	31.1	0.042	0.353
	Inferior frontal gyrus, triangular part_L	157.5	131.6	86.4	100.4	0.044	0.353
	Middle frontal gyrus_L	220.5	159.9	128.6	141.0	0.047	0.353
Temporal	Temporal pole: superior temporal gyrus_L	26.1	32.8	63.3	73.1	0.033	0.353
Parietal	Precuneus_R	654.5	253.5	493.4	273.6	0.046	0.353
Occipital	Superior occipital gyrus_R	15.5	17.7	50.2	83.8	0.049	0.353
Subcortical	Thalamus_R	104.6	108.5	214.0	221.6	0.032	0.353
	Thalamus_L	60.6	63.0	120.6	117.5	0.037	0.353
CC**							
	Median cingulate gyrus_R	0.32	0.06	0.26	0.05	0.003	0.074
	Rolandic operculum_R	0.68	0.25	0.45	0.34	0.016	0.164
Frontal	Inferior frontal gyrus, opercular part_R	0.29	0.24	0.46	0.29	0.035	0.226
	Paracentral lobule_L	0.72	0.28	0.52	0.36	0.047	0.226
Temporal	Temporal pole: superior temporal gyrus_L	0.44	0.25	0.29	0.20	0.035	0.226
Parietal	Cuneus_L	0.41	0.13	0.29	0.14	0.003	0.074
	Cuneus_R	0.49	0.20	0.35	0.11	0.007	0.097
	Angular gyrus_R	0.43	0.15	0.33	0.16	0.039	0.226
Occipital	Inferior parietal lobule_R	0.58	0.23	0.42	0.27	0.047	0.226
	Middle occipital gyrus_R	0.46	0.16	0.35	0.11	0.007	0.097
	Superior occipital gyrus_L	0.54	0.24	0.40	0.16	0.016	0.164
	Calcarine fissure_L	0.35	0.08	0.28	0.13	0.043	0.226
							Continues

Table 3. Continued

Indices	Regions	Control		MMD		P value	q value
		Mean	SD	mean	SD		
Subcortical	Caudate_R	0.33	0.08	0.26	0.06	0.003	0.074
	Thalamus_R	0.51	0.12	0.41	0.14	0.020	0.183
	Putamen_L	0.36	0.08	0.31	0.06	0.035	0.226

BC*: Between-ness centrality; CC**: local cluster coefficient.

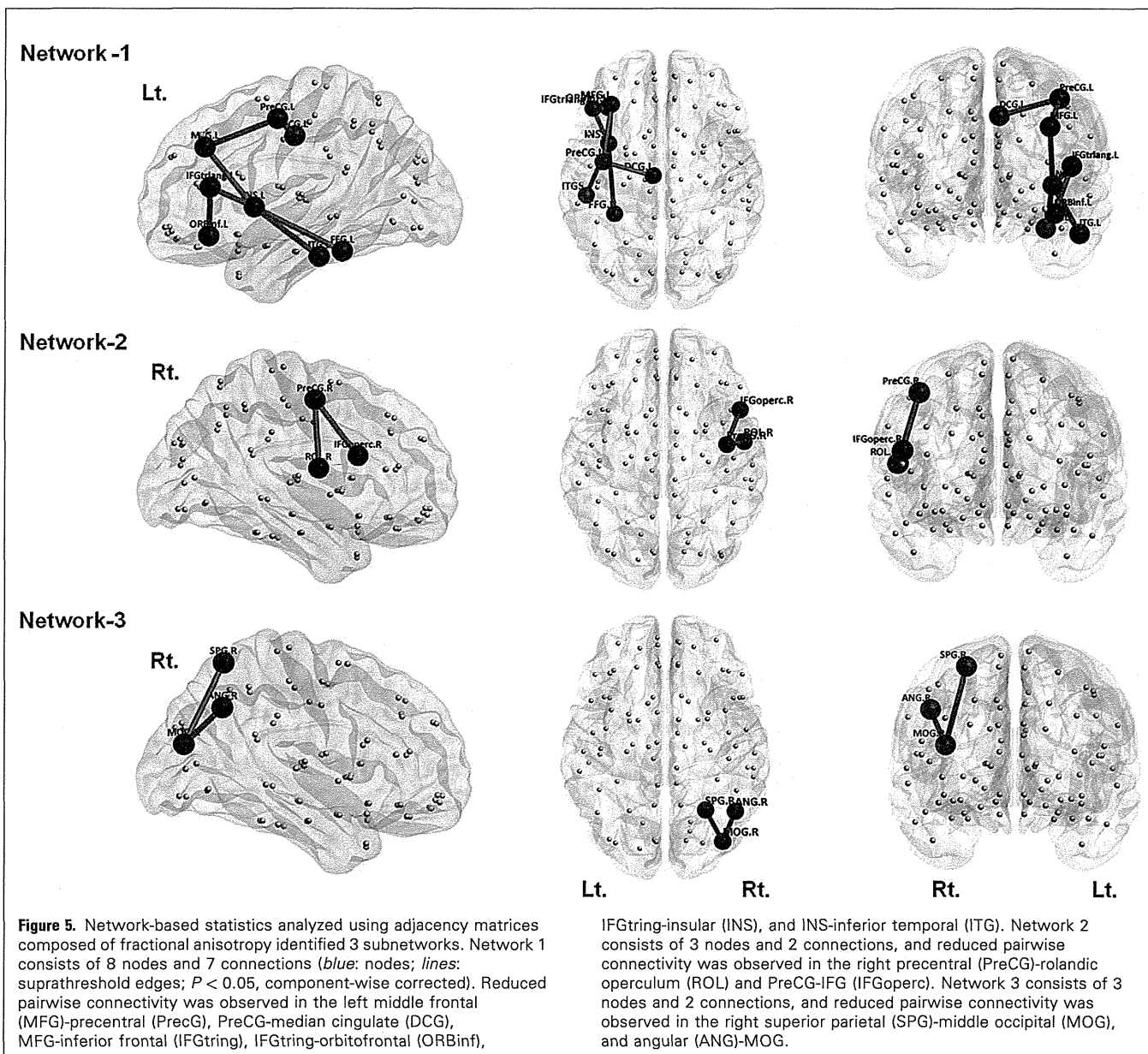


Table 4. Network-Based Statistics Reveals Group Difference between Controls and Moyamoya disease

Subnetwork	Region 1	Region 2	T value	P value
Network 1	Precentral gyrus_L	Middle frontal gyrus_L	3.17	< 0.001
	Inferior frontal gyrus, triangular part_L	Middle frontal gyrus, orbital part_L	3.3	< 0.001
	Middle frontal gyrus_L	Insular_L	3.47	< 0.001
	Inferior frontal gyrus, triangular part_L	Insular_L	3.59	< 0.001
	Precentral gyrus_L	Median cingulate gyrus_L	3.15	< 0.001
	Insular_L	Fusiform gyrus_L	3.21	< 0.001
	Insular_L	Inferior temporal gyrus_L	3.11	< 0.001
Network 2	Precentral gyrus_R	Inferior frontal gyrus, opercular part_R	3.69	< 0.001
	Precentral gyrus_R	Rolandic operculum_R	3.12	< 0.001
Network 3	Middle occipital gyrus_R	Superior parietal gyrus_R	3.69	< 0.001
	Middle occipital gyrus_R	Angular gyrus_R	3.44	< 0.001

attention were selectively affected. The investigation expands our knowledge with respect to overall brain architecture, as well as the neural substrates underlying cognitive dysfunction in patients with MMD.²⁴

Interpretations of Graph Theoretical Measurements

Graph theoretical analysis provides metrics that indicate segregation and integration of distant cortical regions.¹¹ We found the small world property in both control subjects and patients with MMD; however, this property was reduced in patients with MMD. The decline of the small world property is attributed to a decrease in local segregation with preserved global integration, indicating changes toward more random organization in the overall brain network. Brain network organization has been extensively studied in Alzheimer disease, schizophrenia, and multiple sclerosis.¹⁵ Despite their differences in pathology, these diseases demonstrate similar patterns of global network changes, namely increased path length.¹⁵ In contrast to this observation in other disease states, the decline in the global cluster coefficient and a small-world topology with reduced characteristic path length may be a unique network configuration in patients with MMD. Furthermore, reduced degree and BC in the MFG and precuneus are consistent with vulnerability of network nodes with high connectivity (i.e., hubs).^{11,25}

Although reduced regional cerebral blood flow and impaired cognitive function show a strong predilection for the frontal lobe, no specific WM pathways have been identified in association with vascular cognitive impairment secondary to MMD.^{2,26,27} Here, we identified the MFG; insular, dorsal cingulate cortex; and premotor cortex as core structures that undergo network reorganization in patients with MMD. The MFG is connected with the frontopolar region, supplementary motor area, premotor cortex, and IFG by intralobar short range U-shaped tracts and comprises the frontal longitudinal system as an extension of the superior longitudinal fasciculus.²⁸ Previous study using task-induced functional MRI revealed 2 distinct networks, including frontoparietal and cingulo-

opercular components,²⁹ which are considered to participate independently in goal-directed behavior.³⁰ The frontoparietal network consists of the dorsolateral prefrontal cortex, inferior parietal lobe, dorsal frontal cortex, inferior parietal sulcus, precuneus, and middle cingulate cortex. The cingulo-opercular network includes the anterior prefrontal cortex, anterior insula/frontal operculum, dorsal anterior cingulate cortex/medial superior frontal cortex, and thalamus.³⁰ The frontoparietal network is activated when initiating tasks, while the cingulo-opercular network is activated during stable maintenance of a task.³⁰ A recent study using resting-state functional MRI isolated the salience network (SN) from the executive network, which is associated with the identification of cognitively relevant events so as to guide flexible behavior.³¹ Network-based statistical analysis in the present study revealed that networks 1 and 2 partly or entirely include regions such as middle frontal gyrus (MFG), insular, operculum, and dorsal cingulum. These regions are core nodes of either the executive or salience networks. Network 1 included connections that could be associated with executive dysfunction (MFG-precentral), attention deficit, and impaired working memory. Although a smaller number of regions was identified as exhibiting reduced connections in the right hemisphere, we speculate that Network 2 represents portions of the cingulo-opercular network. However, we were not able to find functional associations for Network 3 because there is no known neuropsychologic impairment attributable to the occipital regions in adult MMD.

Clinical Applications

Graph theoretical analysis can be performed using structural (T1, DTI) and functional (resting state or task-enforced functional) MRI data. Various graph-theoretical metrics can demonstrate the organization of brain networks, which could predict current or future cognitive impairment in chronic ischemia. In this study, however, none of the global network measures was correlated with the neuropsychologic examination scores. Impaired connections would affect neurocognition to differing degrees. The lack of

correlations suggests that weighting of specific connections may be necessary. Nevertheless, we speculate that graph metrics can serve as imaging markers for longitudinally tracking the integrity of whole brain organization within patients. In particular, preoperative and postoperative evaluations using graph metrics may shed light on the mechanisms underlying cognitive changes associated with revascularization surgery.

Limitations

First, DTI and deterministic tractography have been applied in previous clinical investigations,^{15,16} but the method for calculating interregional connectivity is not well established.^{12,19,32} Additionally, DTI is hampered by crossing and kissing of fibers when attempting to reconstruct multiple diffusion orientations in single voxels. Second, U fibers connecting adjacent gyri have also been speculated to be vulnerable in ischemia, but this was not taken into consideration in the current analyses. Third, the most severe limitation lies in the definition of interregional connectivity. Previous studies have used binarization of connectivity matrices with a cut-off value of 3 for the number of tract fibers when using deterministic tractography. While this approach eliminates spurious tracts from the analysis, the approach does not take into account subtle alterations in WM tracts with abundant fibers. In addition, adjusting the number of edges in the connection matrix (wiring cost) between patients and controls should be considered in group comparisons.³³ However, applying the same number of edges in a matrix consisting of FA values leads to a disregard of subtle reductions in FA values observed in MMD patients.²

Therefore we applied a threshold to the connectivity matrix to generate a binary matrix, which led us to identify consistent relationships between patients with MMD and controls. Nevertheless, our results should be interpreted as preliminary because the differences did not reach significant level at all threshold values. Finally, cortico-subcortical parcellation is an issue. It has been a matter of debate whether the lateral prefrontal cortex should be considered unitary or heterogeneous in function,^{34,35} and current approaches for investigating the relationship between neurocognitive performance and network parameters may oversimplify the rather complex nature of brain functioning.

In conclusion, we used graph theoretical analysis to analyze brain networks in patients with MMD. Using this approach, we described whole-brain organization and local connectivity associated with cognitive impairment. Describing changes in brain organization in patients with MMD may be potentially useful for monitoring the progression of their cognitive impairment and understanding the capacity for neuroplasticity.

ACKNOWLEDGMENTS

We thank Keiichi Onoda, Ph.D. (Neuroscience, Neuropsychology, Biological Psychology, and Experimental Psychology, Shimane University, Department of Neurology, Japan,) for assistance with data analysis and writing of the manuscript. We also thank Masahito Yamamoto, Ph.D. (Graduate School of Information Science and Technology, Hokkaido University) for assistance with data analysis.

REFERENCES

- Kuroda S, Houkin K. Moyamoya disease: current concepts and future perspectives. *Lancet Neurol.* 2008;7:1056-1066.
- Kazumata K, Tha KK, Narita H, Kusumi I, Shichinohe H, Ito M, et al. Chronic ischemia alters brain microstructural integrity and cognitive performance in adult moyamoya disease. *Stroke.* 2015;46:354-360.
- Karzmark P, Zeifert PD, Bell-Stephens TE, Steinberg GK, Dorfman LJ. Neurocognitive impairment in adults with moyamoya disease without stroke. *Neurosurgery.* 2012;70:634-638.
- Festa JR, Schwarz LR, Pliskin N, Cullum CM, Lacritz L, Charbel FT, et al. Neurocognitive dysfunction in adult moyamoya disease. *J Neurol.* 2010;257:806-815.
- Calviere L, Ssi Yan Kai G, Catalaa I, Marlats F, Bonneville F, Larrue V. Executive dysfunction in adults with moyamoya disease is associated with increased diffusion in frontal white matter. *J Neurol Neurosurg Psychiatry.* 2012;83:591-593.
- Diwadkar VA, Carpenter PA, Just MA. Collaborative activity between parietal and dorso-lateral prefrontal cortex in dynamic spatial working memory revealed by fMRI. *Neuroimage.* 2000;12:85-99.
- Mogensen MA, Karzmark P, Zeifert PD, Rosenberg J, Marks M, Steinberg GK, et al. Neuroradiologic correlates of cognitive impairment in adult Moyamoya disease. *AJNR Am J Neuroradiol.* 2012;33:721-725.
- Barbey AK, Koenigs M, Grafman J. Dorsolateral prefrontal contributions to human working memory. *Cortex.* 2013;49:1195-1205.
- Watts DJ, Strogatz SH. Collective dynamics of 'small-world' networks. *Nature.* 1998;393:440-442.
- Bullmore E, Sporns O. Complex brain networks: graph theoretical analysis of structural and functional systems. *Nature Rev.* 2009;10:186-198.
- Rubinov M, Sporns O. Complex network measures of brain connectivity: uses and interpretations. *Neuroimage.* 2010;52:1059-1069.
- van den Heuvel MP, Mandl RC, Stam CJ, Kahn RS, Hulshoff Pol HE. Aberrant frontal and temporal complex network structure in schizophrenia: a graph theoretical analysis. *J Neurosci.* 2010;30:15915-15926.
- He Y, Chen Z, Evans A. Structural insights into aberrant topological patterns of large-scale cortical networks in Alzheimer's disease. *J Neurosci.* 2008;28:4756-4766.
- Lo CY, Wang PN, Chou KH, Wang J, He Y, Lin CP. Diffusion tensor tractography reveals abnormal topological organization in structural cortical networks in Alzheimer's disease. *J Neurosci.* 2010;30:16876-16885.
- Griffa A, Baumann PS, Thiran JP, Hagmann P. Structural connectomics in brain diseases. *Neuroimage.* 2013;80:515-526.
- Caeyenberghs K, Leemans A, Leunissen I, Michiels K, Swinnen SP. Topological correlations of structural and functional networks in patients with traumatic brain injury. *Front Hum Neurosci.* 2013;7:726.
- Huang Q, Zhang R, Hu X, Ding S, Qian J, Lei T, et al. Disturbed small-world networks and neurocognitive function in frontal lobe low-grade glioma patients. *PLoS One.* 2014;9:e94095.
- Xu H, Ding S, Hu X, Yang K, Xiao C, Zou Y, et al. Reduced efficiency of functional brain network underlying intellectual decline in patients with low-grade glioma. *Neurosci Lett.* 2013;543:27-31.
- Gong G, He Y, Concha L, Lebel C, Gross DW, Evans AC, et al. Mapping anatomical connectivity patterns of human cerebral cortex using in vivo diffusion tensor imaging tractography. *Cereb Cortex.* 2009;19:524-536.
- Mori S, Crain BJ, Chacko VP, van Zijl PC. Three-dimensional tracking of axonal projections in the brain by magnetic resonance imaging. *Ann Neurol.* 1999;45:265-269.
- Cui Z, Zhong S, Xu P, He Y, Gong G. PANDA: a pipeline toolbox for analyzing brain diffusion images. *Front Human Neurosci.* 2013;7:42.
- Zalesky A, Fornito A, Bullmore ET. Network-based statistic: identifying differences in brain networks. *Neuroimage.* 2010;53:1197-1207.

23. Benjamini Y, Hochberg Y. Controlling the false discovery rate: a practical and powerful approach to multiple testing. *J R Stat Soc Series B State Methodol.* 1995;57:289-300.
24. van den Heuvel MP, Sporns O. Rich-club organization of the human connectome. *J Neurosci.* 2011;31:15775-15786.
25. Sporns O, Honey CJ, Kotter R. Identification and classification of hubs in brain networks. *PLoS One.* 2007;2:e1049.
26. Pfefferbaum A, Adalsteinsson E, Sullivan EV. Frontal circuitry degradation marks healthy adult aging: evidence from diffusion tensor imaging. *Neuroimage.* 2005;26:891-899.
27. Black S, Gao F, Bilbao J. Understanding white matter disease: imaging-pathological correlations in vascular cognitive impairment. *Stroke.* 2009;40(suppl 3):S48-S52.
28. Catani M, Dell'acqua F, Vergani F, Schlaggar BL, Petersen SE. Short frontal lobe connections of the human brain. *Cortex.* 2012;48:273-291.
29. Dosenbach NU, Fair DA, Cohen AL, Schlaggar BL, Petersen SE. A dual-networks architecture of top-down control. *Trends Cogn Sci.* 2008;12:99-105.
30. Dosenbach NU, Fair DA, Miezin FM, Cohen AL, Wenger KK, Dosenbach RA, et al. Distinct brain networks for adaptive and stable task control in humans. *Proc Natl Acad Sci U S A.* 2007;104:11073-11078.
31. Menon V, Uddin LQ. Saliency, switching, attention and control: a network model of insula function. *Brain Struct Funct.* 2010;214:655-667.
32. Hagmann P, Sporns O, Madan N, Cammoun L, Pienaar R, Wedeen VJ, et al. White matter maturation reshapes structural connectivity in the late developing human brain. *Proc Natl Acad Sci U S A.* 2010;107:19067-19072.
33. Fornito A, Zalesky A, Breakspear M. Graph analysis of the human connectome: promise, progress, and pitfalls. *Neuroimage.* 2013;80:426-444.
34. Tanji J, Hoshi E. Role of the lateral prefrontal cortex in executive behavioral control. *Physiol Rev.* 2008;88:37-57.
35. Petrides M, Tomaiuolo F, Yeterian EH, Pandya DN. The prefrontal cortex: comparative architectonic organization in the human and the macaque monkey brains. *Cortex.* 2012;48:46-57.

Conflict of interest statement: The authors have no personal or institutional financial interest in the drugs and imaging modalities described herein.

This study was supported by a grant from the Research Committee on moyamoya disease, sponsored by the Ministry of Health (grant number: H27-078), Labor, and Welfare of Japan (Ken Kazumata, Hideo Shichinohe, Masaki Ito, Haruto Uchino, and Takeo Abumiya) This work was also supported by Creation of Innovation Centers for Advanced Interdisciplinary Research Areas Programs, Ministry of Education, Culture, Sports, Science and Technology, Japan (Khin Khin Tha). The sponsors had no role in study design, collection, analysis, or interpretation of data, writing of the report, or decision to submit the paper for publication.

Received 31 August 2015; accepted 30 November 2015

Citation: World Neurosurg. (2016).

http://dx.doi.org/10.1016/j.wneu.2015.11.100

Journal homepage: www.WORLDNEUROSURGERY.org

Available online: www.sciencedirect.com

1878-8750/\$ - see front matter © 2016 Elsevier Inc.

All rights reserved.

SUPPLEMENTARY MATERIAL

Patients

Patients with MMD in the study were diagnosed with MMD according to diagnostic criteria and the guidelines for MMD outlined by the Research Committee on Spontaneous Occlusion of the Circle of Willis (Research Committee on the Pathology and Treatment of Spontaneous Occlusion of the Circle of Willis). Inclusion criteria included the following: 1) >20 years of age, 2) no apparent neurologic deficit due to stroke, and 3) no comorbid illness that affected cognitive function. Exclusion criteria included the following: 1) quasi-moyamoya syndrome with conditions such as Down syndrome or neurofibromatosis and 2) cerebral infarctions >8 mm.

Assessment of the Neurocognitive Function

The interval between the neuropsychological tests and MRI was <1 month. The WAIS-III provides the index scores for overall intellectual ability (full-scale IQ; fIQ), verbal IQ, and motor IQ. Four index scores representing major components of intelligence such as verbal Comprehension Index (VC), perceptual reasoning index (PR), working memory index (WM), and processing speed index (PS) were also used in cognitive assessments. The WCST measures the ability for strategic planning, organized search, and utilization of environmental feedback to shift cognitive sets.¹ Three indicators were calculated, including categories achieved (CA), perseverative errors in Milner (PEM), and Nelson (PEN). The Trail Making Test, Parts A and B assess the speed of information processing and executive functioning, respectively. The time to complete TMT-A and TMT-B was measured, and the differences in score between TMT-A and TMT-B (B-A) were calculated. The CPT measures a person's sustained and selective attention and impulsivity. The reaction time (RT) and number of omission errors were measured. The Stroop test measures sustained attention. A reaction time delay was examined in naming the color of the word printed in an unmatched color. The RST is a complex verbal test, which evaluates both storage and processing (i.e., reading) elements of working memory.² The scores are expressed as the total number and proportion of words correctly recalled. We used cut-off values to classify patients on the basis of neuropsychologic tests described in the previous article.³

Scan Parameters

T1-weighted, sagittal, 3-dimensional, magnetization-prepared rapid acquisition gradient echo sequences that covered the entire brain (128 slices, slice thickness 1.33 mm, repetition time [TR] 2530 ms, echo time [TE] 3.39 ms, inversion time 1100 ms, flip angle 7°, acquisition matrix 256 × 256, field of view [FOV] 256 × 256 mm², average 1) were acquired. Diffusion tensor images were acquired using a single-shot echoplanar imaging sequence that covered the whole brain (49 axial slices, slice thickness 2.5 mm with no interslice gap, TR 7200 ms, TE 104 ms, flip angle 90°, 32 diffusion directions with b 1000 s/mm², and an additional image without diffusion weighting [i.e., b 0 s/mm²], acquisition matrix 128 × 128, FOV 230 × 230 mm², average 1).

Preprocessing Imaging Data

Data preprocessing included eddy current and motion artifact correction of DTI data, calculation of the diffusion tensor, and estimation of the probabilistic distribution of fiber orientations for each voxel. Eddy current distortions and motion artifacts in the DTI dataset were corrected by applying affine alignment of each diffusion-weighted image to the b 0 image. After this, the diffusion tensor elements were estimated by solving the Stejskal and Tanner equation, and then the reconstructed tensor matrix was diagonalized to obtain 3 eigenvalues (1, 2, and 3) and eigen vectors. The probabilistic distribution of fiber orientations for each voxel was estimated with a 2-tensor model.^{4,5}

Construction of Connectivity Matrix

A whole-brain fiber tracking was performed using the fiber assignment by continuous tracking streamline tractography algorithm in the Diffusion toolkit (<http://www.trackvis.org/>).^{6,7} Stop angle threshold was set to 35°. Anatomic parcellation was performed using automated anatomic labeling (AAL).⁸ A linear transformation was applied within each subject's DTI image (b = 0) and T1-weighted image. The individual T1-weighted image was then nonlinearly registered to the ICBM 152 template (Montreal Neurological Institute). Then, the inverse transformation matrix was obtained and applied to the AAL template in standard space. Ninety cortical and subcortical ROIs were used for constructing the connectivity matrix. The whole-brain tractography described earlier yields several parameters representing connectivity in each pair of nodes across 90 brain regions. An adjacency matrix was obtained by averaging FA by the volume of the fiber tract connecting region. Construction of connectivity matrices was performed in MATLAB R2012b (Mathworks, Natick, USA) and an open-source pipeline package (<http://www.nitrc.org/projects/panda/>).⁹

Parameters of Graph Theoretical Analysis

Global networks are characterized by parameters associated with integration (Eg; global efficiency, L; characteristic path length, λ); segregation (Ei; local efficiency, Ci; modularity, CC; cluster coefficient, γ; normalized cluster coefficient); and architecture (C, σ; small-world property, Hubs). The clustering coefficient is the number of connections that exist between the nearest neighbors of a node as a proportion of the maximum number of possible connections.¹⁰ The characteristic path length (L) is the average shortest path, where path represents the minimum number of edges that must be traversed to go from one node to another.¹⁰ Global efficiency (Eg) is the inverse of path length (L).¹⁰ A network with high clustering (CC) in a relatively low diameter (L) is referred to as a small world (σ).¹⁰ In the present study, the clustering coefficient, characteristic path length, normalized clustering coefficient (γ = CC/CC rand), and characteristic path length (λ = L/Lrand) were computed, where Crand and Lrand represent the average weighted clustering coefficient and shortest path length of 100 surrogate random networks with preserved edge weights. Modularity (Ci) quantifies the degree to which the network may be subdivided into delineated groups.¹⁰ Ci is calculated by maximizing the number of edges in a subgroup and minimizing the number of edges between subgroups.

Degree, local clustering coefficient, and between-ness centrality (BC) were calculated to examine the local network characteristics of each brain region in the structural network.¹⁰ Degree indicates the number of edges in the graph. BC is the fraction of all shortest

paths in the network that contain a given node.¹⁰ Nodes with high BC values participate in a large number of shortest paths. A detailed description regarding the data analysis using DTI and graph theory has been provided in previous literature.^{6,11}

REFERENCES

1. Monchi O, Petrides M, Petre V, Worsley K, Dagher A. Wisconsin Card Sorting revisited: distinct neural circuits participating in different stages of the task identified by event-related functional magnetic resonance imaging. *J Neurosci*. 2001;21:7733-7741.
2. Hupet M, Desmette D, Schelstraete MA. What does Daneman and Carpenter's reading span really measure? *Percept Mot Skills*. 1997;84:603-608.
3. Kazumata K, Khin Tha K, Narita H, Kusumi I, Shichinohe H, Ito M, et al. Chronic ischemia alters brain microstructural integrity and cognitive performance in adult moyamoya disease. *Stroke*. 2015;46:354-360.
4. Behrens TE, Berg HJ, Jbabdi S, Rushworth MF, Woolrich MW. Probabilistic diffusion tractography with multiple fibre orientations: what can we gain? *Neuroimage*. 2007;34:144-155.
5. Behrens TE, Woolrich MW, Jenkinson M, Johansen-Berg H, Nunes RG, Clare S, et al. Characterization and propagation of uncertainty in diffusion-weighted MR imaging. *Magn Reson Med*. 2003;50:1077-1088.
6. Gong G, He Y, Concha L, Lebel C, Gross DW, Evans AC, et al. Mapping anatomical connectivity patterns of human cerebral cortex using in vivo diffusion tensor imaging tractography. *Cereb Cortex*. 2009;19:524-536.
7. Mori S, Crain BJ, Chacko VP, van Zijl PC. Three-dimensional tracking of axonal projections in the brain by magnetic resonance imaging. *Ann Neurol*. 1999;45:265-269.
8. Tzourio-Mazoyer N, Landeau B, Papathanassiou D, Crivello F, Etard O, Delcroix N, et al. Automated anatomical labeling of activations in SPM using a macroscopic anatomical parcellation of the MNI MRI single-subject brain. *Neuroimage*. 2002;15:273-289.
9. Cui Z, Zhong S, Xu P, He Y, Gong G. PANDA: a pipeline toolbox for analyzing brain diffusion images. *Front Hum Neurosci*. 2013;7:42.
10. Rubinov M, Sporns O. Complex network measures of brain connectivity: uses and interpretations. *Neuroimage*. 2010;52:1059-1069.
11. Xu Y, Qiu S, Wang J, Liu Z, Zhang R, Li S, et al. Disrupted topological properties of brain white matter networks in left temporal lobe epilepsy: a diffusion tensor imaging study. *Neuroscience*. 2014;279:155-167.